ELSEVIER

Nuclear Instruments and Methods in Physics Research B 201 (2003) 114–122

NIM B
Beam Interactions with Materials & Atoms

www.elsevier.com/locate/nimb

Angular distribution of X-ray radiation by 500 MeV electrons in a tungsten crystal

Y.N. Adischev [a,*], S.N. Arishev [a], A.V. Vnukov [a], A.V. Vukolov [a], A.P. Potylitsyn [a], S.I. Kuznetsov [a], V.N. Zabaev [b], B.N. Kalinin [b], V.V. Kaplin [b], S.R. Uglov [b], A.S. Kubankin [c], N. Nasonov [c]

[a] *Tomsk Polytechnik University, 30 Lenin Avenue, 634034 Tomsk, Russia*
[b] *Nuclear Physics Institute of Tomsk Polytechnik University, 2a Lenin Avenue, 634050 Tomsk, Russia*
[c] *Laboratory of Radiation Physics, Belgorod State University, 14 Studencheskaya strasse, 308007 Belgorod, Russia*

Received 14 March 2002; received in revised form 27 June 2002

Abstract

X-rays generated by a 500 MeV electron beam of the Tomsk synchrotron in a tungsten single crystal with a mosaic factor less than 80″ has been studied theoretically and experimentally. The tungsten crystal was a block with sizes $1.7 \times 10 \times 15$ mm^3 aligned with the (1 1 1) plane at the Bragg angle $\theta_B \approx 45°$ to the electron beam axis. The emitted photons were detected at an angle of $2\theta_B$ with respect to the electron beam. The emitted angular distributions for the (2 2 2) and (4 4 4) orders have been measured and compared with predictions of the developed theoretical model. This model takes the contribution of parametric X-radiation (PXR) and diffracted transition radiation (DTR) generated by relativistic electrons from in-surface of a crystalline target as well as an influence of an interference between PXR and DTR emission mechanisms into account. The obtained results show the important contribution of DTR to the measured emission yield.

PACS: 78.70.−g; 78.70.Ck; 79.90.+t
Keywords: X-ray emission; Dynamical diffraction; Photon spectra; Emission angular distribution

1. Introduction

Crystals of perfect crystallographic structure and large atomic numbers, such as tungsten, are used for producing of intense fluxes of highly directed quasi-monochromatic gamma-quanta on the basis of relativistic electron channeling radiation [1,2]. Currently the perfect tungsten crystal is considered as the most appropriate radiator in the positron source based on the channeling radiation [3–5]. The bent perfect tungsten crystal can be used as the deflector for an extraction of charged particles (including heavy ions) from high energy circular accelerators by channeling effect [6]. It should be noted that the extraction efficiency is

* Corresponding author.
E-mail address: adischev@interact.phtd.tpu.edu.ru (Y.N. Adischev).

0168-583X/02/$ - see front matter
PII: S0168-583X(02)01310-1

considerably more for heavy deflector than for light one.

The new possible application of perfect tungsten crystals is connected with quasi-monochromatic tunable X-ray beam producing on the basis of the parametric X-rays (PXR) from relativistic electrons in a crystal [7–9]. PXR cross-section increases proportional to Z^2 when increasing of the crystal atomic number Z. But an absorption length decreases proportional to Z^{-4}, therefore it is difficult to make the most of indicated advantage of heavy crystals for gain in PXR source efficiency. In addition to this within the range of high enough emitting particle energies $\gamma \gg \gamma_*$ (γ is the Lorentz factor of an emitting particle, $\gamma_* = \omega_B/\omega_0$, ω_B is the Bragg frequency, in the vicinity of which PXR spectrum is concentrated, ω_0 is the plasma frequency of the crystal) the width of PXR angular distribution $\Delta\Theta \sim \gamma_*^{-1}$ exceeds essentially due to the density effect [10] the width of primary particles equilibrium electromagnetic field in a vacuum $\Delta\Theta \sim \gamma^{-1}$ This effect decreases dramatically PXR angular density.

On the other hand it is in the range of high emitting particle energies $\gamma > \gamma_*$ the diffracted transition radiation (DTR) contributes to the total emission yield [11]. DTR appears due to the scattering of a fast particle transition radiation emitted from in-surface of the crystal by precisely the same atomic planes of this crystal giving rice to PXR manifestation. Since DTR angular width is identical with that for transition radiation ($\Delta\Theta \sim \gamma^{-1}$) its angular density can exceed PXR one very essentially in the range $\gamma \gg \gamma_*$. It is important that DTR is formed at the small distance of the order of the extinction length $l_{ext} \sim \omega_B/\omega_0^2$. This circumstance opens the possibility to create an effective X-ray source consisting of a stack of thin crystals with thickness in the region of l_{ext} placed along an emitting particle trajectory at the distance greater that an emission formation length in a vacuum [12].

It seems likely that DTR has been observed for the first time at the Darmstadt accelerator S-DALINAC [13]. The light crystal of Si(1 1 1) and 86.9 MeV electron beam have been used in this experiment. The main goal of our work is to search experimentally the relationship between DTR and PXR in the emission process of 500 MeV electrons crossing the heavy perfect crystal as W(1 1 1) when the difference between PXR and DTR angular distributions is much more pronounced in accordance with theoretical predictions. The measurements are supplemented by the detailed theoretical analysis of emission process based in X-ray dynamical diffraction theory [14].

In Section 3 X-ray emission from relativistic electrons incident on semi-infinite absorbing crystal is considered theoretically. Such model analogous to that in [11] is adequate to the conditions of our experiment because the thickness of used W-target exceeds essentially an absorption length. Separate contributions of PXR and DTR as well as an interference between these emission mechanisms are analyzed in this work in contrast with [11]. Such approach has been used earlier [15] but without account of the influence of a beam divergence, photon collimator size and photoabsorption, considered in this work. Setup and experimental conditions are outlined in Section 2. The comparison of obtained experimental results with theoretical predictions is performed in this section as well. Some concluding remarks are presented in Section 4.

2. Experiment

The experimental schematic used is shown in Fig. 1. Electrons accelerated in vacuum chamber were incident on internal tungsten target. The incidence time was 15 ms and frequency 5 Hz.

The tungsten crystal was a block with size $1.7 \times 10 \times 15$ mm^3 manufactured by the method of zone melting with subsequent grinding and etching. The large face of the crystal coincided with the (1 1 1) plane to an accuracy less than 30′, the mosaic factor as low 80″. The spectral and angular characteristics were measured by an X-ray Cd–Te spectrometer with the energy resolution 1 keV for 13, 95 and 17, 8 keV L-lines of Am^{241} isotope. Detector angular size $\theta_B \approx 2.5 \times 10^{-3}$ rad. The number of accelerated electrons was monitored by an induction current pickup and by a synchrotron radiation counter. The number of electrons passing through the target was determined

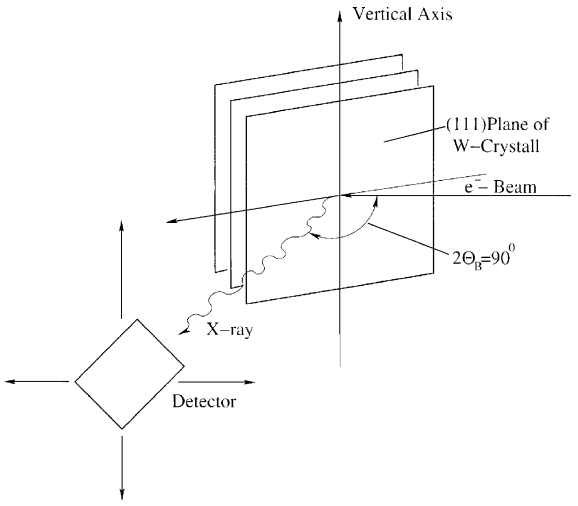

Fig. 1. Experimental schematic.

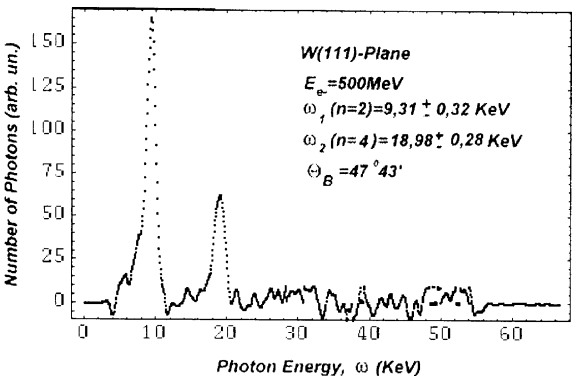

Fig. 2. The spectrum of X-ray radiation from W-crystal target.

by measuring the total energy by Wilson quantometer.

In the course of measurements, the accelerated current was maintained at a level, when the spectrometer loading was less than 2×10^2 photon/accelerator pulse.

The crystal was aligned with the plane (1 1 1) at the Bragg angle $\theta_B \approx 45°$ to the electron beam direction by a goniometer with the angular step 2×10^{-5} rad for the vertical 7×10^{-6} rad for horizontal axis rotation, respectively. The photons were detected at $2\theta_B \approx 90°$ with respect to the electron beam.

Fig. 2 depicts the spectrum of X-radiation from the tungsten crystal obtained within this geometry with the electron energy 500 MeV.

The spectrum exhibits a characteristic peaks at the photon energies $\omega_{(222)}$ and $\omega_{(444)}$ corresponding to the first and second orders of PXR according to the Bragg relation:

$$\omega = \frac{\pi hcn}{d \sin \theta_B}, \quad n = 1, 2, 3, \tag{1}$$

where d is interplane spacing, n-order of diffraction.

In Figs. 3 and 4 is shown angular distributions of X-ray yield for horizontal and vertical planes for (2 2 2) and (4 4 4) orders of diffraction and $\theta_B \approx 47°3'$.

These measurements have revealed that the angular distributions of the X-ray radiation from electrons in the crystal differ substantially from those for pure PXR or DTR. Figs. 5 and 6.

3. Theoretical description

Let us consider an emission from relativistic electrons crossing a boundary of a semi-infinite absorbing crystal with reflecting crystallographic plane parallel to the surface of a target (see Fig. 1, where $\mathbf{e}_1$ is the axis of an electron beam, g is the reciprocal lattice vector determining the reflecting plane). The solution of the wave equation

$$(k^2 - \omega^2(1+\chi_0))\mathbf{E}_{\omega\mathbf{k}} - \mathbf{k}(\mathbf{k}\mathbf{E}_{\omega\mathbf{k}}) - \omega^2 \sum_{\mathbf{g}}{}' \chi_{-\mathbf{g}} \mathbf{E}_{\omega\mathbf{k}+\mathbf{g}} = \frac{\mathrm{i}\omega e}{2\pi^2} \mathbf{v}\delta(\omega - \mathbf{k}\mathbf{v}), \tag{2}$$

where $\mathbf{v}$ is the velocity of an emitting particle, $\mathbf{E} = (2\pi)^{-4} \int \mathrm{d}t\, \mathrm{d}^3 r \mathbf{E}(\mathbf{r}t) \mathrm{e}^{\mathrm{i}\omega t - \mathrm{i}\mathbf{k}\mathbf{r}}$ is the Fourier-transform of the electric field $\mathbf{E}$, coefficients χ_0 and $\chi_\mathbf{g}$ determine the crystal dielectric permeability $\epsilon(\omega, \mathbf{r}) = 1 + \chi_0(\omega) + \sum_\mathbf{g}' \chi_\mathbf{g}(\omega) \mathrm{e}^{\mathrm{i}\mathbf{g}\mathbf{r}}$, can be found within the frame of typical for PXR description two-wave approximation of the dynamical diffraction theory [14]

$$\begin{aligned} &(k^2 - \omega^2(1+\chi_0))E_{\lambda 0} - \omega^2 \chi_{-\mathbf{g}} \alpha_\lambda E_{\lambda\mathbf{g}} \\ &\quad = \frac{\mathrm{i}\omega e}{2\pi^2} \mathbf{e}_{\lambda 0} \mathbf{v}\delta(\omega - \mathbf{k}\mathbf{v}), \\ &((\mathbf{k}+\mathbf{g})^2 - \omega^2(1+\chi_0))E_{\lambda\mathbf{g}} - \omega^2 \chi_\mathbf{g} \alpha_\lambda E_{\lambda 0} = 0, \end{aligned} \tag{3}$$

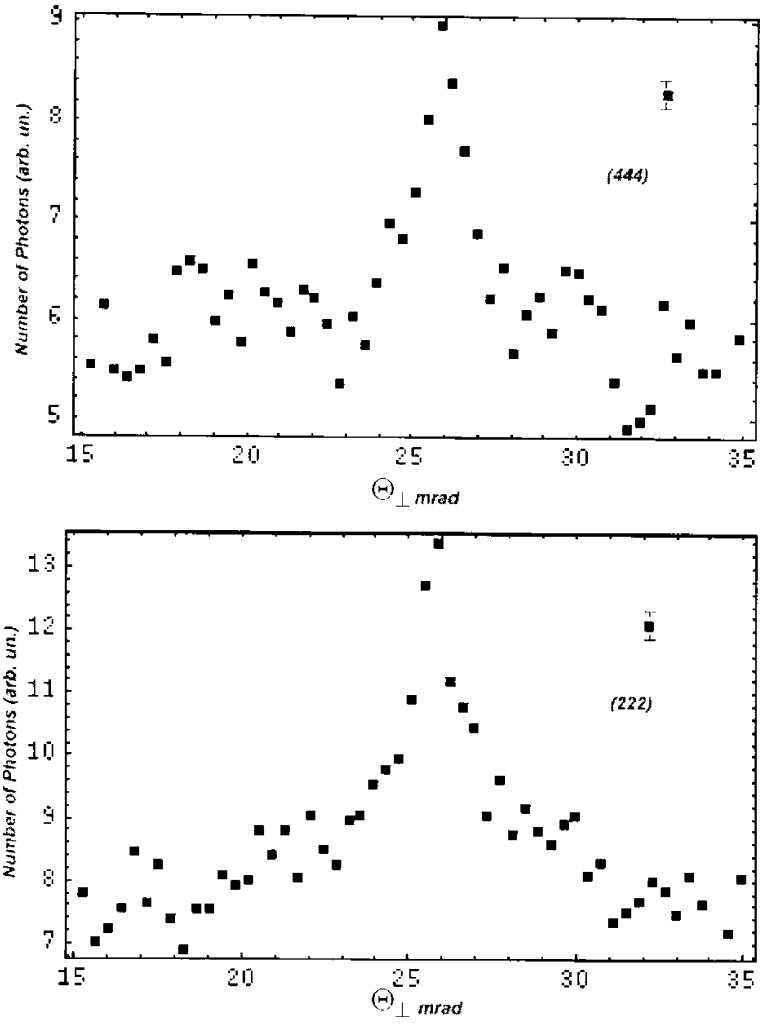

Fig. 3. Angular distribution of the intensity of X-radiation (horizontal plane).

where the following definitions are used:

$$\mathbf{E}_{\omega\mathbf{k}} = \sum_{\lambda=1}^{2} \mathbf{e}_{\lambda 0} E_{\lambda 0}, \quad \mathbf{E}_{\omega\mathbf{k}+\mathbf{g}} = \sum_{\lambda=1}^{2} \mathbf{e}_{\lambda\mathbf{g}} E_{\lambda\mathbf{g}},$$
$$\mathbf{e}_{10} \sim [\mathbf{k}\mathbf{g}], \quad \mathbf{e}_{1\mathbf{g}} = \mathbf{e}_{10}, \quad \mathbf{e}_{20} \sim [\mathbf{k}_1, \mathbf{e}_{10}],$$
$$\mathbf{e}_{2\mathbf{g}} \sim [\mathbf{k}+\mathbf{g}, \mathbf{e}_{10}]. \tag{4}$$

Unit vectors $\mathbf{e}_{\lambda 0}$ and $\mathbf{e}_{\lambda\mathbf{g}}$ in (2) and (3) are the polarization vectors, $\alpha_1 = 1$, $\alpha_2 = \cos\varphi$ (see Fig. 1).

Eq. (3) describes the field inside the crystal. The relevant equations for the field in a vacuum outside the crystal follow from (3) in the limit χ_0, $\chi_{\mathbf{g}}$, $\chi_{-\mathbf{g}} \to 0$. In particular the emission field in a vacuum $E^{\mathrm{v}}_{\lambda\mathbf{g}}$ of interest to us is described by the equation

$$(k_{\mathbf{g}}^2 - \omega^2) E^{\mathrm{v}}_{\lambda\mathbf{g}} = 0, \tag{5}$$

where $\mathbf{k}_g = \mathbf{k} + \mathbf{g}$. The solution of this equation

$$E^{\mathrm{v}}_{\lambda\mathbf{g}} = a_\lambda(\mathbf{k}_\parallel)\delta(k_{gx} - p), \quad p = \sqrt{\omega^2 - k_\parallel^2},$$
$$\mathbf{k}_\parallel = \mathbf{k}_g + \mathbf{k}_z \tag{6}$$

contains the unknown coefficient a_λ. To determine this coefficient one should use the corresponding solution of Eq. (3) and the ordinary boundary conditions for field components at the crystal

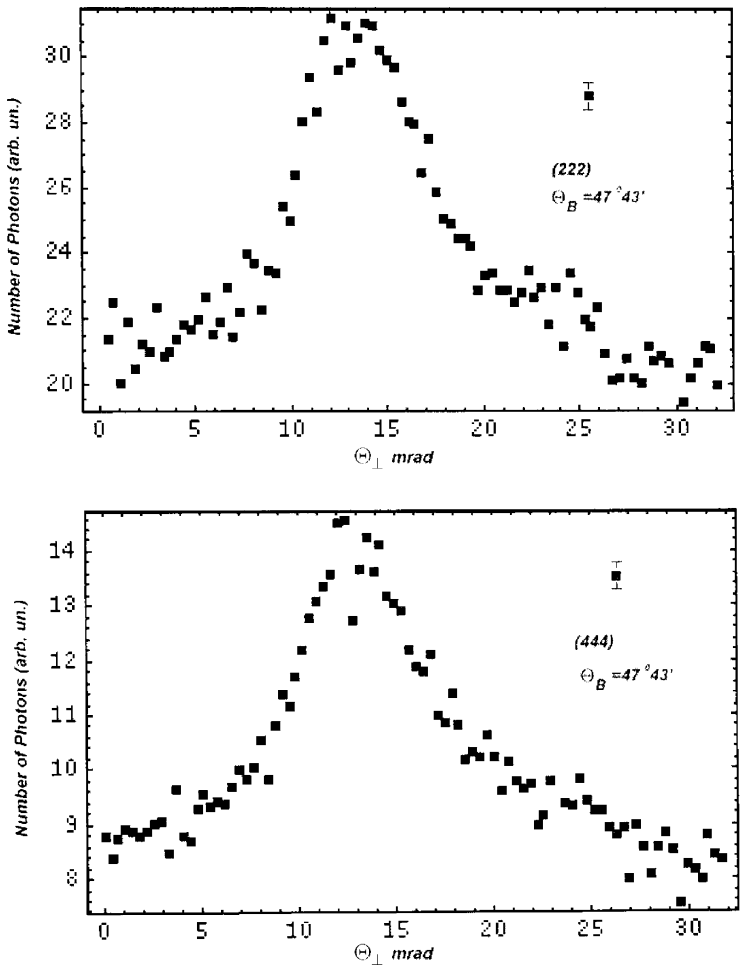

Fig. 4. Angular distribution of the intensity of X-radiation (vertical plane).

surface. The following expression for a_λ can be derived as a result of simple manipulations

$$a_\lambda = \frac{i\omega^3 e\chi_{\mathbf{g}}\alpha_\lambda}{8\pi^2 p|v_x|}\frac{\mathbf{e}_{\lambda 0}}{\xi_* - \frac{\omega^2}{2\pi}\chi_0}\left(\frac{1}{\Delta-\xi_0}+\frac{\xi_0-\xi_*}{(\xi_0-\xi_1)(\xi_0-\xi_2)}\right),$$
$$\xi_0 = \frac{1}{v_x}(\omega - \mathbf{k}_\parallel\mathbf{v} + pv_x) + \Delta,\quad \Delta = g\left(\frac{g}{2p}-1\right) \ll g,$$
$$\xi_{1,2} = \frac{1}{2}\left(\Delta \pm \sqrt{\left(\Delta - \frac{\omega^2}{p}\chi_0\right)^2 - \frac{\omega^4}{p^2}\chi_{\mathbf{g}}\chi_{-\mathbf{g}}\alpha_\lambda^2}\right). \tag{7}$$

In the case of Bragg scattering geometry under consideration the quantity ξ_* is defined by the formulae

$$\xi_* = \xi_1,\quad \text{if } \Delta > \frac{\omega^2}{p}\mathrm{Re}\left[\chi_0 + \sqrt{\chi_{\mathbf{g}}\chi_{-\mathbf{g}}}|\alpha_\lambda|\right],$$
$$\xi_* = \xi_2,\quad \text{if } \Delta < \frac{\omega^2}{p}\mathrm{Re}\left[\chi_0 + \sqrt{\chi_{\mathbf{g}}\chi_{-\mathbf{g}}}|\alpha_\lambda|\right]. \tag{8}$$

Calculation of the Fourier integral $E_\lambda^{\mathrm{Rad}} = \int \mathrm{d}^3 k_{\mathbf{g}} E^v_{\lambda\mathbf{g}} \mathrm{e}^{i\mathbf{k}_{\mathbf{g}}r}$ allows one to derive the radiation pulse height A_λ,

$$E_\lambda^{\mathrm{Rad}} = \int \mathrm{d}^3 k_{\mathbf{g}} E^v_{\lambda\mathbf{g}} \mathrm{e}^{i\mathbf{k}_{\mathbf{g}}\mathbf{n}r} \to A_\lambda \frac{\mathrm{e}^{i\omega r}}{r},$$
$$A_\lambda = -2\pi i\omega n_x a_\lambda(\omega\mathbf{n}_\parallel), \tag{9}$$

where $\mathbf{n} = \mathbf{n}_\parallel + \mathbf{n}_x$ is the unit vector along the direction of emitted photon propagation, $\mathbf{n}_\parallel \mathbf{n}_x = 0$.

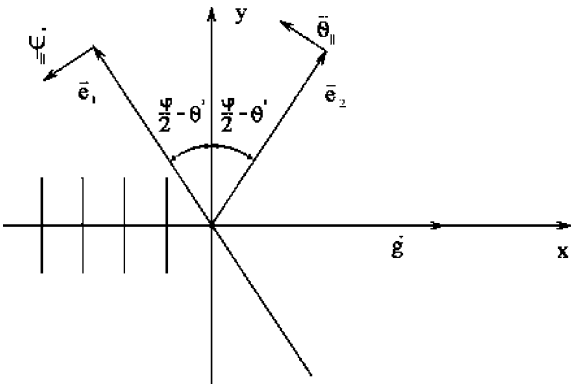

Fig. 5. Bragg scattering geometry for the considered task, $\mathbf{e_1}$ is the axis of an electron beam, $\mathbf{e_2}$ is the axis of emitted photon flux, θ' is the orientation angle, φ is the fixed emission angle, $\Psi_\parallel$ and $\Theta_\parallel$ are the components of the angles $\mathbf{\Psi}$ and $\mathbf{\Theta}$ describing the angular distributions of emitting electrons and emitted photons, respectively.

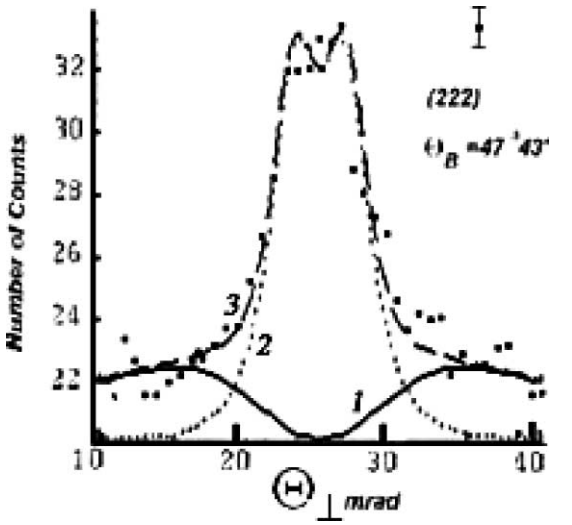

Fig. 6. Angular distribution of emitted photons in vertical plane, the curve 1 describes PXR distribution, curve 2 describes DTR distribution, the curve 3 corresponds to the total emission distribution, points correspond to the measured angular distribution of the total emission.

Formulae (7)–(9) provide a complete description of spectral-angular characteristics of radiation. For further analysis it is more convenient to rearrange the expression for the radiation pulse height, using the simplest approximation for susceptibilities,

$$\chi_0 = -\frac{\omega_0^2}{\omega^2} + i\chi_0'', \qquad \chi_{\mathbf{g}} = \chi_{-\mathbf{g}} = -\frac{\omega_{\mathbf{g}}^2}{\omega^2} + i\chi_{\mathbf{g}}'', \quad (10)$$

where $\omega_{\mathbf{g}}^2 = \omega_0^2(F(g)/Z)(S(\mathbf{g})/N_0)\mathrm{e}^{-\frac{1}{2}g^2u^2}$, $F(g)$ is the atom formfactor, $S(\mathbf{g})$ is the structure factor of an elementary cell, containing N_0 atoms, u is the r.m.s. amplitude of thermal vibrations of atoms. Let us introduce into consideration 2-D variables $\mathbf{\Psi}$ and $\mathbf{\Theta}$ describing by the formulae

$$\mathbf{v} = \mathbf{e}_1\left(1 - \frac{1}{2}\gamma^{-2} - \frac{1}{2}\Psi^2\right) + \mathbf{\Psi}, \quad \mathbf{e}_1\mathbf{\Psi} = 0,$$
$$\mathbf{n} = \mathbf{e}_2\left(1 - \frac{1}{2}\Theta^2\right) + \mathbf{\Theta}, \quad \mathbf{e}_2\mathbf{\Theta} = 0, \quad \mathbf{e}_1\mathbf{e}_2 = \cos\varphi, \quad (11)$$

the e-beam divergence and the angular distribution of emitted photons (see Fig. 1).

Formulae (7)–(11) allow to obtain the following expression for the total emission spectral-angular distribution:

$$\omega\frac{\mathrm{d}N_\lambda}{\mathrm{d}\omega\,\mathrm{d}^2\theta} = \left\langle\left|A_\lambda^{\mathrm{PXR}} + A_\lambda^{\mathrm{DTR}}\right|^2\right\rangle,$$
$$A_\lambda^{\mathrm{PXR}} = \frac{e}{\pi}\delta_\lambda\frac{\Omega_\lambda}{\gamma^{-2}+\gamma_*^{-2}+\Omega^2} \times \frac{1}{\tau + \mathrm{sign}(\tau-\delta_\lambda\kappa_\lambda)f_\lambda' - \sigma - \mathrm{i}f_\lambda''},$$
$$A_\lambda^{\mathrm{DTR}} = \frac{e}{\pi}\delta_\lambda\Omega_\lambda\left(\frac{1}{\gamma^{-2}+\Omega^2} - \frac{1}{\gamma^{-2}+\gamma_*^{-2}+\Omega^2}\right) \times \frac{1}{\tau + \mathrm{sign}(\tau-\delta_\lambda\kappa_\lambda)f_\lambda' - \mathrm{i}(\eta + f_\lambda'')}, \quad (12)$$

where $\delta_\lambda = \omega_{\mathbf{g}}^2|\alpha_\lambda|/\omega_0^2$, $\Omega_1 = \Theta_\perp - \Psi_\perp$, $\Omega_2 = 2\theta' + \Theta_\parallel + \Psi_\parallel$, $\Omega^2 = \Omega_1^2 + \Omega_2^2$, $\eta = \omega^2\chi_0''/\omega_0^2$, $\kappa_\lambda = \chi_{\mathbf{g}}''|\alpha_\lambda|/\chi_0''$, the brackets $\langle\ \rangle$ mean the averaging over the angles $\Psi_\perp$ and $\Psi_\parallel$, the important quantities $\tau(\omega)$, σ, f_λ', f_λ'' are defined by the formulae

$$\tau(\omega) = \frac{g^2}{2\omega_0^2}\left(1 - \frac{\omega}{\omega_{\mathrm{B}}'}\right), \quad \omega_{\mathrm{B}}' = \omega_{\mathrm{B}}\left[1 + (\theta' + \Theta_\parallel)\cot\frac{\varphi}{2}\right],$$
$$\sigma = \gamma_*^2(\gamma^{-2} + \gamma_*^{-2} + \Omega^2), \quad \omega_{\mathrm{B}} = \frac{g}{2\sin\frac{\varphi}{2}},$$
$$f_\lambda'^{,''} = \frac{1}{\sqrt{2}}\sqrt{\sqrt{(\tau^2-\delta_\lambda^2)^2 + 4\pi\eta^2(\tau-\delta_\lambda\kappa_\lambda)^2} \pm (\tau^2 - \delta_\lambda^2)}. \quad (13)$$

Let us use the obtained results (12) and (13) to analyze the relative contributions from the side of PXR and DTR to total emission yield. First, let us consider DTR properties. The simple formula

$$\omega\frac{\mathrm{d}N\lambda^{\mathrm{DTR}}}{\mathrm{d}\omega\,\mathrm{d}^2\Theta} = \frac{e^2}{\pi^2}\left\langle \Omega_\lambda^2\left(\frac{1}{\gamma^{-2}+\Omega^2}-\frac{1}{\gamma^{-2}+\gamma_*^{-2}+\Omega^2}\right)^2\right\rangle R_\lambda^{\mathrm{DTR}},$$

$$R_\lambda^{\mathrm{DTR}} = \frac{\delta_\lambda^2}{\left(\tau+\mathrm{sign}(\tau-\delta_\lambda\kappa_\lambda)f_\lambda'\right)^2+\left(\eta+f_\lambda''\right)^2}, \tag{14}$$

following from (12) clearly indicates the nature of DTR as Bragg reflected transition radiation emitted from a relativistic electron crossing the in-surface of the crystal R_λ^{DTR} is the reflection coefficient.

In accordance with (14) DTR angular distribution coincides practically with that of transition radiation. Particularly, the width of DTR angular distribution is determined by the energy of emitting particle and coincides with that for the field of virtual photons associated with a relativistic particle moving in a vacuum $\Delta\Theta\sim\gamma^{-1}$.

It should be noted that the dependence of the distribution (14) on the energy of emitted quantum ω is concentrated in the non-dimensional variable $\tau(\omega)$. Since $R_\lambda^{\mathrm{DTR}}\approx 1$ in the range $|\tau|<\delta\lambda$ and $R_\lambda^{\mathrm{DTR}}\sim\tau^{-2}$ if $|\tau|\gg\delta_\lambda$ (ordinary behavior of X-ray dynamical reflection coefficient) the spectral width of DTR has the very small value $\Delta\omega/\omega\sim 2(\omega_0^2/g^2)\Delta\tau\sim\omega_0^2/g^2\ll 1$. The performed numerical analysis of the formula (14) has shown a weak dependence of DTR distribution on the parameters η and κ_λ within the range of small photoabsorption ($\eta\ll 1$). Assuming the coefficients η and κ_λ in (14) to be equal to zero one can integrate (14) over energies of emitted photons and obtain the very simple expression for DTR angular distribution,

$$\frac{\mathrm{d}N_\lambda^{\mathrm{DTR}}}{\mathrm{d}^2\Theta} = \frac{16e^2\omega_0^2}{3\pi^2g^2}\delta_\lambda\left\langle \Omega_\lambda^2\left(\frac{1}{\gamma^{-2}+\Omega^2}-\frac{1}{\gamma^{-2}+\gamma_*^{-2}+\Omega^2}\right)^2\right\rangle, \tag{15}$$

which can be used for explanation of experimental results.

Returning to the general formula (12) let us consider the separate PXR contribution. The formula for PXR spectral-angular distribution

$$\omega\frac{\mathrm{d}N_\lambda^{\mathrm{PXR}}}{\mathrm{d}\omega\,\mathrm{d}^2\Theta} = \frac{e^2}{\pi^2}\left\langle\frac{\Omega_\lambda^2}{\left(\gamma^{-2}+\gamma_*^{-2}+\Omega^2\right)^2}R_\lambda^{\mathrm{PXR}}\right\rangle,$$

$$R_\lambda^{\mathrm{PXR}} = \frac{\delta_\lambda^2}{\left(\tau+\mathrm{sign}(\tau-\delta_\lambda\kappa_\lambda)f_\lambda'-\sigma\right)^2+\left(f_\lambda''\right)^2}, \tag{16}$$

shows clearly that PXR appears due to the scattering of the screened Coulomb field of a relativistic particle. It is important that PXR photons are emitted from the whole thickness of a target therefore PXR yield is proportional to the absorption length $l_{\mathrm{ab}}\approx(f_\lambda'')^{-1}$ in the case of semi-infinite crystal under consideration. Since $f_\lambda''\ll 1$ due to the inequality $\eta\ll 1$ the quantity R_λ^{PXR} considered as a function of τ has a strong maximum at the point $\tau_*\approx(\sigma^2+\delta_\lambda^2)/2\sigma>\delta_\lambda$ following from the equation $\tau_*+f_\lambda'(\tau_*)-\sigma=0$. Using the well known approximation $(x^2+\alpha^2)^{-1}\approx(\pi/\alpha)\delta(x)$ if $\alpha\ll 1$ one can obtain from (16) after integration over ω the following expression for PXR angular distribution:

$$\frac{\mathrm{d}N_\lambda^{\mathrm{PXR}}}{\mathrm{d}^2\Theta} = \frac{e^2\omega_0^2}{\pi g^2}\frac{\delta_\lambda^2}{\eta} \times\left\langle\frac{\Omega_\lambda^2}{\left(\gamma^{-2}+\gamma_*^{-2}+\Omega^2\right)^2+\gamma_*^{-4}\delta_\lambda^2-2\kappa_\lambda(\gamma^{-2}+\gamma_*^{-2}+\Omega^2)\gamma_*^{-2}\delta_\lambda} \times\left(1-\frac{\gamma_*^{-4}\delta_\lambda^2}{\left(\gamma^{-2}+\gamma_*^{-2}+\Omega^2\right)^2}\right)^2\right\rangle, \tag{17}$$

Obviously in the region of low energies of emitting particles $\gamma\ll\gamma_*$ the expression (17) is reduced to well-known formula of PXR kinematic theory [16]. One of the most notable new effects appearing in the region of dynamic scattering $\gamma\gg\gamma_*$ is that of anomalous photoabsorption (Borrmann's effect) in PXR, which follows from (17) for strong reflections ($\delta_\lambda\approx 1$) in the frequency range where $\kappa_\lambda\approx 1$ (the last condition coincides with that of Borrmann effect manifestation in free X-ray scattering in a crystal). This effect consisting in the shift of PXR angular maximum to the side

of small observation angles and essential growth of its amplitude has been considered in detail in work [17] and is beyond the scope of this paper.

Let us briefly discuss the influence of an interference between the pulse heights A_λ^{PXR} and A_λ^{DTR} on the total emission yield. The expression

$$\omega\frac{\mathrm{d}N_\lambda^{\mathrm{INT}}}{\mathrm{d}\omega\,\mathrm{d}^2\Theta}=\frac{e^2}{\pi^2}\left\langle\frac{\Omega_\lambda^2}{\gamma^{-2}+\gamma_*^{-2}+\Omega^2}\left(\frac{1}{\gamma^{-2}+\Omega^2}-\frac{1}{\gamma^{-2}+\gamma_*^{-2}+\Omega^2}\right)R_\lambda^{\mathrm{INT}}\right\rangle,$$

$$R_\lambda^{\mathrm{INT}}=\frac{2}{\delta_\lambda^2}R_\lambda^{\mathrm{PXR}}R_\lambda^{\mathrm{DTR}}\left[(\tau+\mathrm{sign}(\tau-\delta_\lambda\kappa_\lambda)f_\lambda')\times(\tau+\mathrm{sign}(\tau-\delta_\lambda\kappa_\lambda)f_\lambda'-\sigma)+f_\lambda''(\eta+f_\lambda'')\right],\tag{18}$$

following from (12) describes this interference effect quantitatively.

According to (14), (16) and (18), PXR predominates in the region of kinematic diffraction $\gamma\ll\gamma_*$, while the contributions from DTR and the interference term can be neglected. In the region of dynamic scattering $\gamma\gg\gamma_*$, where both DTR and PXR contributions are essentially large, the interference effect is still negligible. This occurs due to substantially different angular distributions of the emitted quanta of the respective emission mechanisms (DTR photons are concentrated mainly within the observation angle range $\Omega\approx\gamma^{-1}$ according to the formula (15), while the angular distribution maximum for PXR lies in the region of much larger angles $\Omega\approx\gamma^{-1}$ as it follows from (17)). The expression for R_λ^{INT} in (18) is a direct indication of the small value of the interference term in the region $\tau\approx\tau_*$, where the major PXR contribution is centered. In the region $|\tau|<\delta_\lambda$, where the DTR contribution predominates, the interference term is small compared to (14).

Thus the simple formulae (15) and (17) give the complete description of discussed emission angular and orientation characteristics. Let us use these formulae to calculate certain of such characteristics measured in our experiment. Since experimentally the value of Bragg angle $\theta_{\mathrm{B}}=\varphi/2$ was very close to 45°, only DTR and PXR components corresponding to the polarization index $\lambda=1$ can make an essential contribution to total emission yield, as it follows at once from the expression (15) and (17) containing the coefficient $\delta_\lambda\sim\alpha_\lambda$ (on condition $\varphi/2\approx45^\circ$ the coefficient $\alpha_2=\cos\varphi$ is close to zero). Under these conditions DTR and PXR angular densities are proportional to $\Theta_\perp^2$ in accordance with (15) and (17). Therefore the yield of collimated photon flux measured in horizontal plane ($\Theta_\perp=0$) is small and depends strongly on both the X-ray detector angular size and the accuracy of the condition $\Theta_\perp=0$ implementation. On this basis we have calculated for the comparison with experimental results the emission angular distribution in vertical plane ($\theta'=0$, see Fig. 1). The curves presented in Fig. 2 have been calculated by (15) and (17) with the understanding that the reflecting plane was (2 2 2), $\gamma=10^3$, electron beam angular spread $\theta_0=10^{-3}$ rad, X-ray detector unregular size $\theta_{\mathrm{d}}=2.510^{-3}$ rad. Since experimental data have been obtained in arbitrary units the theoretical curve 3 describing the total emission yield was normalized to data in one experimental point.

4. Conclusions

The study of this work clarify the physical nature of X-ray emission mechanism determining the characteristics of a photon flux emitted from relativistic electrons passing through heavy crystals aligned so that the Bragg geometry for the electron equilibrium electromagnetic field scattering by the crystal can be realized.

The derived simple formulae describing the emission spectral-angular and angular distributions show that the total emission yield is formed by the contribution of PXR and DTR. The interference between these emission mechanisms is negligibly small. According to obtained theoretical results in the range of high enough emitting particle energies $\epsilon\gg\epsilon_*=m\omega_{\mathrm{B}}/\omega_0$ (m is the electron mass, ω_{B} is the Bragg frequency, ω_0 is the plasma frequency) the main contribution to an emission angular distribution is given by DTR, therefore the width of this distribution is close to γ^{-1}. PXR contribution shapes the wide background in the range of large observation angles.

Acknowledgement

This work was supported in part by RFBR (grant: 00-02-16388).

References

[1] C.Yu. Amosov, B.N. Kalinin, G.A. Naumenko, A.P. Potylitsin, V.P. Sarythev, I.S. Tropin, I.E. Vnukov, in: Yu.L. Pivovarov, A.P. Potylitsin (Eds.), Proceeding of the International Symposium on Radiation of Relativistic Electrons in Periodical Structures, Tomsk, 1993.
[2] G.L. Bochek, V.I. Kulibaba, N.I. Maslov, V.D. Ovchinnik, B.I. Shramenko, Nucl. Instr. and Meth. B 145 (1998) 146.
[3] B.N. Kalinin, G.A. Naumenko, A.P. Potylitsin, V.A. Versilov, I.E. Vnukov, K. Matsukado, T. Takashima, T. Takahashi, H. Okuno, K. Nakagama, Nucl. Instr. and Meth. B 145 (1998) 209.
[4] V.N. Baier, A.D. Bukin, T.V. Dimova, V.P. Druzhinin, M.S. Dubrovin, V.B. Golubev, S.I. Serednyakov, V.V. Shary, V.M. Strakhovenko, X. Artru, M. Chevallier, R. Kirsh, J.-C. Poitat, J. Major, A.P. Potylitsin, I.E. Vnukov, Nucl. Instr. and Meth. B 145 (1998) 221.
[5] M. Inone, O. Takenaka, K. Yoshida, I. Endo, M. Iinuma, T. Takahashi, A.V. Bogdanov, A.M. Kolchuzhkin, A.P. Potylitsin, I.E. Vnukov, H. Okuno, S. Anami, A. Enomoto, K. Furukawa, T. Kamitani, Y. Ogawa, S. Ohsawa, Nucl. Instr. and Meth B 173 (2001) 111.
[6] A.S. Artem'ev, V.V. Boiko, A.D. Kovalenko, A.M. Taratin, JINR Communications, NR1-99-12V, Dubna, 1999.
[7] M.L. Ter-Mikaelian, High-Energy Electromagnetic Processes in Condensed Media, Wiley, New York, 1972.
[8] G.M. Garibian, C. Yang, Sov. Phys. J. Exp. Theor. Phys. 34 (1972) 495.
[9] V.G. Baryshevsky, I.D. Feranchuk, Sov. Phys. J. Exp. Theor. Phys. 34 (1972) 502.
[10] N.N. Nasonov, A.G. Safronov, in: Yu.L. Pivovarov, A.P. Potylitsin (Eds.), Proceeding of the International Symposium in Radiation of Relativistic Electrons in Periodical Structures, Tomsk, 1993.
[11] A. Caticha, Phys. Rev. B 45 (1992) 9541.
[12] N. Nasonov, Phys. Lett. A 246 (1998) 148.
[13] J. Freudenberger, H. Genz, V.V. Morokhovskii, I. Reitz, A. Richter, in: Abstracts of International Workshop on radiation Physics with Relativistic Electrons, 9–12 June 1998, Tabart, Germany.
[14] Z. Pinsker, Dynamical Scattering of X-rays in Crystals, Springer, Berlin, 1984.
[15] X. Artru, P. Rullhusen, Nucl. Instr. and Meth B 145 (1998) 1.
[16] I.D. Feranchuk, A.I. Ivashin, J. Phys. (Paris) 46 (1985) 1981.
[17] C.K. Gary, V.V. Kaplin, N.N. Nasonov, M.A. Piestrup, S.R. Uglov, Yad. Fizika 64 (2001) 1.